**Proceedings of the ASME 2010 3rd Joint US-European Fluids Engineering Summer Meeting and
8th International Conference on Nanochannels, Microchannels, and Minichannels
FEDSM-ICNMM2010
August 1-5, 2010, Montreal, Canada**

FEDSM-ICNMM2010-30813

THREE DIMENSIONAL VOLUMETRIC VELOCITY MEASUREMENTS IN THE INNER PART OF A TURBULENT BOUNDARY LAYER OVER A ROUGH WALL USING DIGITAL HPIV

Siddharth Talapatra
Johns Hopkins University,
Baltimore, MD, USA

Joseph Katz
Johns Hopkins University,
Baltimore, MD, USA

ABSTRACT

Microscopic digital Holographic PIV is used to measure the 3D velocity distributions in the roughness sublayer of a turbulent boundary layer over a rough wall. The sample volume extends from the surface, including the space between the tightly packed, 0.45 mm high, pyramidal roughness elements, up to about 5 roughness heights away from the wall. To facilitate observations though a rough surface, experiments are performed in a facility containing fluid that has the same optical refractive index as the acrylic rough walls. Magnified in line holograms are recorded on a 4864×3248 pixel camera at a resolution of 0.67µm/pixel. The flow field is seeded with 2µm silver coated glass particles, which are injected upstream of the same volume. A multiple-step particle tracking procedure is used for matching the particle pairs. In recently obtained data, we have typically matched ~5000 particle images per hologram pair. The resulting unstructured 3D vectors are projected onto a uniform grid with spacing of 60 µm in all three directions in a 3.2×1.8×1.8 mm sample volume. The paper provides sample data showing that the flow in the roughness sublayer is dominated by slightly inclined, quasi-streamwise vortices whose coherence is particularly evident close to the top of the roughness elements.

INTRODUCTION

Surface roughness effects are apparent in most practical wall bounded flows such as flows over turbine blades, ship hulls and aircrafts, as well as pipeline and geophysical flows (Raupach , [1], Jimenez, [2], Rotach, [3]). The flow within the roughness sublayer, i.e. within 2-5 roughness heights away from the surface, is inherently complicated and depends on the local geometry. Resolving this flow is vital to bridge the gap between flow conditions at the surface, especially the shear stress, and the outer layer flows. Of special interest are the coherent structures forming in the near-wall region and the manner in which they are affected by roughness. These structures impact the wall shear stress, and their evolution is directly related to the turbulence production (e.g. Aubrey et al. [4]). Because of technical challenges in measuring the flow within the roughness sublayer, there is very little data on the flow and turbulence there, except for some qualitative flow visualizations (e.g. Grass [5]) and turbulent stresses based on single point measurements (Krogstad et al. [6]). Two-Dimensional PIV measurements in the same facility and flow conditions of the present paper have been reported recently by Hong et al. ([7], [8]). These data complement the present measurements of volumetric 3D velocity distributions using Digital Holographic microscopic PIV (DHM PIV). Recent DNS studies have provided detailed description of the near-wall flow structure, but typically at low Reynolds numbers, and 2D roughness geometry (e.g. Ikeda & Durbin, [9], Ashrafian et al., [10], Leonardi et al., [11]).

A key modeling issue for rough wall boundary layers is to determine the extent up to which the roughness influences the turbulence in the boundary layer. The Townsend's 1976 wall similarity hypothesis, as extended by Raupach [10], states that at sufficiently high Re, turbulent motions become independent of wall roughness outside the roughness sublayer. This outer layer similarity has been supported (e.g. Nakagawa & Hanratty, [12], Flack et al., [13], Wu & Christensen, [14]) and disputed (e.g. Krogstad & Antonia, [15]) by different experimental studies. As reasoned by Jimenez [2], two conditions must be satisfied for the different studies to be comparable, and to identify asymptotic effects of wall roughness on the outer layer: First, there must be sufficient scale separation between roughness and boundary layer dimensions, and second, the flow should be fully rough. The following conditions are required: $\delta/k \geq 50$ and $k^+ \geq 80$, where δ is the boundary layer thickness, k is the roughness height, and k^+ is its wall unit normalized value. In the current experiments, the roughness geometry and the channel flow parameters are set to satisfy both conditions. Indeed, Hong et al. [8] show that spatial variations in Reynolds stress statistics associated with roughness geometry are

confined to the lowest two roughness heights away from the wall. However, small scale turbulent structures generated near the wall persist over the entire boundary layer.

Performing volumetric 3D measurements near a rough wall is a major challenge, and to the best of our knowledge such data does not exist today. This paper illustrates the principles, the scope and practical issues on making measurements through a rough wall with the motivation of investigating the aforementioned issue. To this end, preliminary results based on some 3D instantaneous velocity fields are presented.

EXPERIMENTAL SETUP

Digital Microscopic Holographic PIV: Holography (Gabor, [16]) comprises of two steps: recording a hologram, either on a photographic film or on a digital sensor; and reconstructing this hologram, either optically or numerically, to obtain the original 3D light field. There are numerous methods for recording a hologram, but they all involve capturing the interference pattern between a reference beam and the light scattered from objects located in the volume of interest. For the current experiments, an inline setup (Fig.1) is utilized, primarily because of the simplicity of the optical setup. The sample volume is illuminated by a collimated beam, which serves both as a reference beam and an illuminating light source. Part of this beam is scattered by objects located in the path of the beam, and interferes with the remaining, undisturbed part of the beam. Since our goal is to perform high resolution measurements of the flow within the roughness sublayer, the interference patterns are magnified using a 10X microscope objective (Sheng et al., [17]).
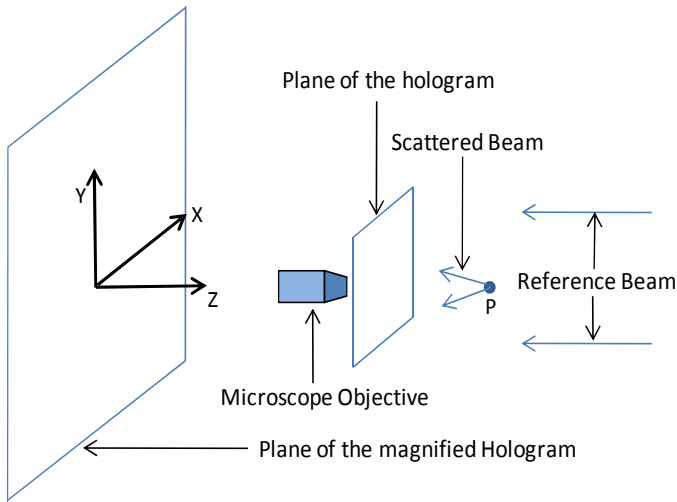

Fig.1 In-line microscopic Holographic Optical Setup: Part of the reference beam is scattered by point object P, and interferes with the rest of the collimated beam to form the Hologram. A microscope objective magnifies the hologram and shifts the plane of the hologram away from the sample volume.

The magnified interference pattern, i.e., the hologram, is recorded on a high-resolution digital sensor, and sent to a computer for numerical reconstruction of the original particle field. This process is performed by convolving the hologram with a kernel that is representative of light field propagating from a point source using the Fresnel Diffraction Formula (Sears, [18], Katz & Sheng, [19]),

$$E(x,y,z) = \iint H(x',y',0) \cdot \frac{e^{ikr}}{r^2} dx'dy',$$

$$r = \sqrt{(x-x')^2 + (y-y')^2 + z^2}, \; k = \frac{2\pi}{\lambda} \quad (1)$$

where x, y and z are the coordinates specified in Fig.1, λ is the wavelength, $E(x, y, z)$ represents the light field, and $H(x, y, 0)$ is the 2D hologram intensity distribution at z = 0, and z represents the distance from the hologram to the reconstructed plane. Since typically $z \gg [(x-x')^2 + (y-y')^2]^{0.5}$, a far field approximation can be applied, modifying the kernel to

$$\frac{e^{ikr}}{r^2} \rightarrow \frac{e^{ikz}}{i\lambda z} e^{i\frac{k}{2z}(x^2+y^2)} \quad (2)$$

The far field approximation becomes

$$E(x,y,z) = H(x,y,0) * \frac{e^{ikz}}{i\lambda z} e^{i\frac{k}{2z}(x^2+y^2)} \quad (3)$$

This convolution can be solved efficiently by using Fast Fourier Transforms. Intensity distributions representing the particle fields are reconstructed at different depths by varying *z*. After reconstruction, data analysis typically involves spatial filtering to remove background noise, e.g. by subtracting the time averaged intensity distribution over many exposures. Next, 3D segmentation is performed to obtain a list of the particles located in the sample volume and their approximate 3D coordinates. Two particle distributions recorded within a small time interval can be used for measuring the 3D velocity field using the particle tracking method described in detail in Sheng et al. [20, 21]. The tracking algorithm utilizes seven different criteria for matching the particle traces in the two exposures, e.g. use of planar PIV analysis to provide a search neighborhood, particle size and depth similarity, similarity with neighboring vectors, etc.

Particle tracking provides an unstructured vector field, which needs to be interpolated along a structured 3D grid in order to compute relevant flow quantities. Fig. 2 shows a 2D projection of the 3D grid system, where P_1, P_2 ...P_N show the locations of unstructured velocity vectors and P_G is a sample grid point. The velocity at each grid point can be extrapolated to all the unstructured points that lie within its selected neighborhood, which is represented by the dotted curve. Using first order approximation, the velocities at each grid is related to the unstructured values using:

$$
\begin{bmatrix} u_1 \\ v_1 \\ w_1 \\ .... \\ w_N \end{bmatrix} = \begin{bmatrix} 1 & 0 & 0 & \Delta x_1 & \Delta y_1 & \ldots & 0 \\ 0 & 1 & 0 & 0 & 0 & \ldots & 0 \\ 0 & 0 & 1 & 0 & 0 & \ldots & \Delta z_1 \\ & & & . & & & \\ & & & . & & & \\ & & & . & \Delta z_n & & \end{bmatrix} \begin{bmatrix} u_G \\ v_G \\ w_G \\ \partial u_G / \partial x \\ \partial u_G / \partial y \\ \partial u_G / \partial z \\ ...... \\ \partial w_G / \partial z \end{bmatrix} \quad (4)
$$

where u_i is the velocity vector at P_i, u_G is the velocity at P_G, and $(\Delta x_i, \Delta y_i, \Delta z_i)$ is the displacement vector from P_i to P_G. The velocity at P_G is obtained by the inverse of eq. (4), which is calculated by using Singular value decomposition (Golub & Loan, [22]). This procedure directly provides the local spatial velocity gradients, but to increase the accuracy of calculated gradients, we use an expanded version of eq. (4), which includes the second order spatial derivatives as well. The latter requires at least 10 unstructured grid points in the neighborhood of each regular grid point. We do not calculate the structured vectors for grid points with fewer unstructured vectors in the specified neighborhood.
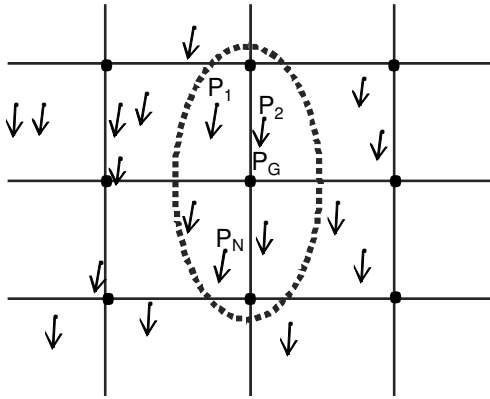

Fig.2 A 2D projection of the grid along with the unstructured, measured velocity vectors. The dotted curve represents a selected neighborhood that is used for calculating the velocity at the regular nodes.

Proof of Concept Tests: The sample volume of interest lies next to a rough surface, which would distort the interference patterns generated by the tracer particles. Consequently, experiments have been performed by matching the optical index of refraction of the working fluid with that of the rough wall. We use a concentrated solution of NaI in water, 62% by weight to match the refractive index of an acrylic wall. In order to verify that we can actually record holograms through the optically index-matched facility, i.e. to ascertain whether slight variations

in the refractive index can render the holograms unusable, preliminary proof of concept experiments were performed. These tests were conducted in an acrylic chamber filled with NaI solution that had a rough surface with the same geometry as that used in the actual experiments. Holograms of the seeded flow field clearly confirmed that we could record and reconstruct the particle field though the rough wall, as well as computes the velocity distribution. We subsequently proceeded to record 3D data in a high Reynolds number boundary layer over a rough wall described in the following section.

Turbulent Channel Experiments: The experiments were performed in a 3.3 m long, acrylic rectangular channel that has a 20×5cm cross-section. This channel is an extension of the JHU optically index-matched facility (Miorini et al., [23]) that uses the abovementioned NaI solution as a working fluid. At a channel centerline velocity of 2.75m/s, the Reynolds number based on centerline velocity and half channel height (h) is $Re_h=62500$, the friction velocity is 0.16m/s, the wall unit is 7μm, and the associated friction velocity Reynolds number is $Re_\tau=3400$, where the wall shear stress is obtained from recent 2D PIV measurements performed in the same facility and conditions (Hong et. al., [7]). Two 1.25m long, rough surfaces of the same properties are inserted symmetrically in the bottom and top walls of the fully developed flow region of the channel. The roughness elements consist of uniformly distributed, closely packed, square pyramids with height of 0.45mm and slope angle of 22°. The pyramids are inclined at 45° to the free stream. The roughness height and channel dimensions yielded h/k=56 and k^+=90, satisfying the required fully rough flow and scale separation conditions, as outlined in the introduction.

Fig. 3 illustrates the flow channel along with the optical arrangement used to record the HPIV data. The light source is a pulsed Nd-Yag Laser (532nm), whose beam is attenuated to produce 1 μJ/pulse. The delay between exposures is 25μs. The beam is spatially filtered and collimated, and passed through the channel rough walls, along the negative Y direction. The interference pattern is then magnified by a 10X objective, and the hologram is recorded on a 4864×3248 pixel camera, as shown in the inset, providing a 3.3×2.2mm field of view with an in-plane resolution of 0.67μm/pixel.

In order to ensure sufficient seeding close to the volume of interest, and to reduce the number of out of focus particles, localized injection of seed particles from the wall is utilized. The injection system consists of 28 holes, 100μm diameter each, drilled 2cm upstream of the field of view between the roughness elements. The 2μm diameter, silver coated glass particles are injected at a concentration of 10^9 particles per ml and a volumetric flow rate of about 0.01ml/s. The resulting injection speed is 0.1 m/s, i.e. 3% of the free stream velocity. These conditions ensure minimal disruption to the flow being measured.

A 1k×1k pixel section of a sample hologram (6% of the total area) is presented in Fig. 4a. Fig. 4b shows a superposition of two corresponding reconstructed images, depth averaged from 300 to 800μm starting at the base of the pyramids. These image

Copyright © 2010 by ASME

sub-sections shown here have a cross section of 0.7×0.7mm. In-focus particle pairs, some of them highlighted by red curves, can be clearly seen.

The primary challenge in this experiment has been ensuring sufficient seeding in the region of interest by varying the parameters of the localized injection system. This problem has been resolved to a significant extent, but further improvements could still be made to obtain optimum seeding consistently. On average, 4000-5000 particle pairs have been detected and tracked to obtain the corresponding 3D velocity vectors in a sample volume of 3.2×1.8×1.8mm, the long dimension being the streamwise direction. The presently available data resolves the flow from 150μm below the peak of the pyramid ($y/k=-0.33$, $y^+=-21.5$) to 1650μm above the peak ($y/k=3.67$, $y^+=235$), hence spanning almost the entire roughness sublayer. Thus, $y=0$ is defined at the pyramid peak. For the present preliminary data, the neighborhood ellipsoidal volume is 300μm long (40 wall units, $0.67k$) in the streamwise direction and 180μm (25 wall units, $0.4k$) in the other two directions. The structured vector spacing is 60μm (8.5 wall units, $0.13k$).
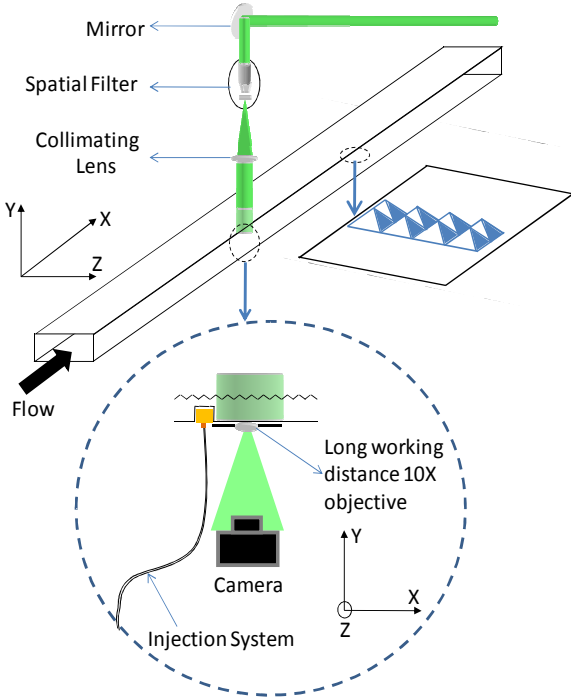

Fig.3 Experimental Setup for the turbulent rough wall channel Experiment. The inset shows the hologram acquisition and injection systems.

3. RESULTS

Currently, 40 pairs of holograms have been analyzed to yield the 3D velocity distributions and associated velocity gradient tensors. This number is insufficient to obtain any meaningful statistics of the flow and turbulence. However, the instantaneous realizations can be utilized to examine flow
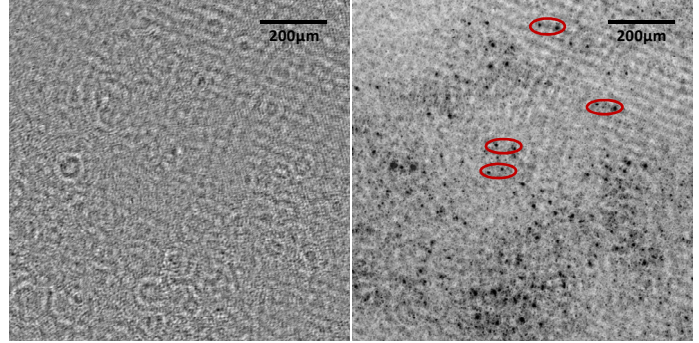

Fig. 4(a) A 1k×1k section of a hologram, (b) Superposition of a pair of reconstructed images, depth averaged over 0.5 mm.

structures over the entire roughness sublayer, including the space between roughness elements.

Fig. 5 shows a sample 3D structured velocity field with mean streamwise velocity subtracted, containing ~3000 vectors, under-sampled from ~15000 vectors. The coordinates shown are relative to a single pyramidal roughness element. The flow can be observed to lift upwards due to blockage imposed by the pyramid, and seems to contain "large" coherent structures in the outer region. Fig. 6a-d show two samples of instantaneous velocity distributions in X-Z planes located at $y/k=0.07$ and 1.27. Each shows vectors of the in-plane velocity components along with contours of the total velocity magnitude. The first plane is located just above the peak of the roughness, and the second is located a little more than one roughness height away from the peak. Both examples, which are representative of the rest of the data, show elongated regions of low and high velocity aligned in the streamwise direction at $y/k=0.07$. The velocity is typically (but not always) low along the ridgeline of the pyramids, i.e. along a line connecting the peaks, and high between ridgelines. Such a channeling phenomenon has also been seen in Hong et al. [7] using X-Z plane 2D PIV data. At $y/k=1.27$, there are still significant spatial variations in velocity, but the streamwise elongated streaks become rare. Almost all the samples analyzed so far show similar trend.

Fig. 7a and b show vectors of instantaneous velocity projections at two different X on Y-Z planes of the same velocity field, superimposed with the streamwise vorticity contour, ω_x. The presence of quasi-streamwise vortices is evident, with some, but not all, persisting in both planes. The vortical structure marked by a + is inclined upward at an angle of 27º. Fig. 8a and b show the streamwise and wall-normal vorticity components distributions projected on a streamwise-spanwise plane, just above the roughness. Regions with high ω_x of both signs (Fig. 8a) typically also have high ω_y (Fig. 8b), indicating that the streamwise vortices are inclined vertically. These vortices are preferentially situated in the high speed channel region, on both sides of the pyramids.

The HPIV data also enables us to visualize the 3D flow structures, e.g. by plotting the iso-surfaces of Q, the second

invariant of the velocity gradient tensor (Hunt et al., [24]). This variable is frequently used for identifying vortical structures. One can also plot vortex lines to show the orientation of 3D vorticity to visualize the effect of coherent structures on vortex lines. Two samples are presented in Figures 9a and b. Essentially all the structures are oriented in the streamwise direction, with some upward lifting, especially along the backward facing sides of the pyramid. The sample vortex lines shown are located close to the wall, and largely oriented in the spanwise direction, but they lift away from the surface, twist and bend under the action of large vortices, roughness induced blockages, and spatial variations in mean flow. For example, the previously mentioned flow channeling accelerates the vortex segments in the elevated speed region between pyramid ridges, and slows down the vortex line elements that are located above the ridge.
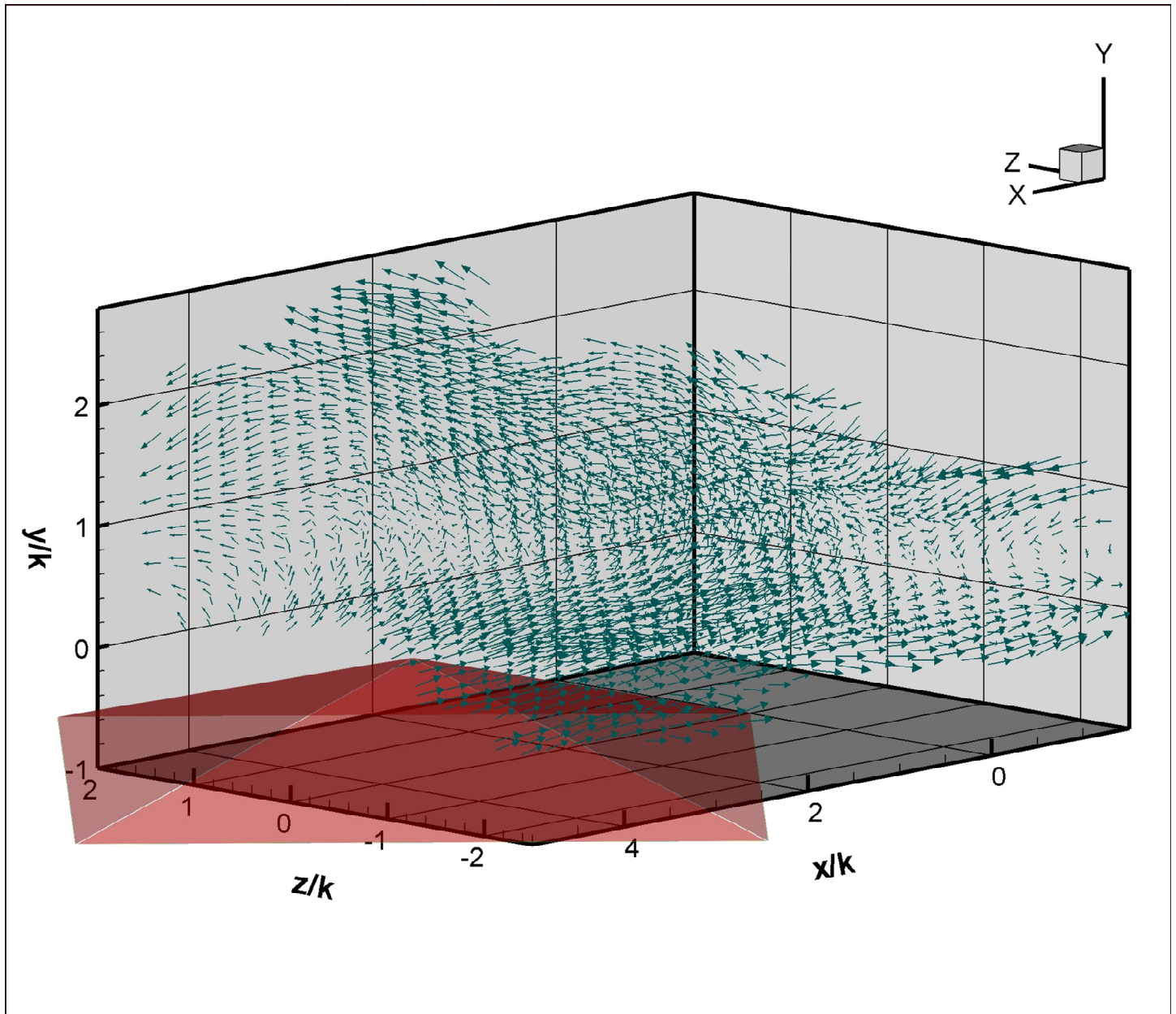

Fig.5 An under-sampled, streamwise mean velocity subtracted, structured 3D velocity distribution. The vectors are plotted at a particular grid point only when there are sufficient unstructured vectors in the neighborhood of that grid point. The coordinate system is relative to a pyramidal element shown here.
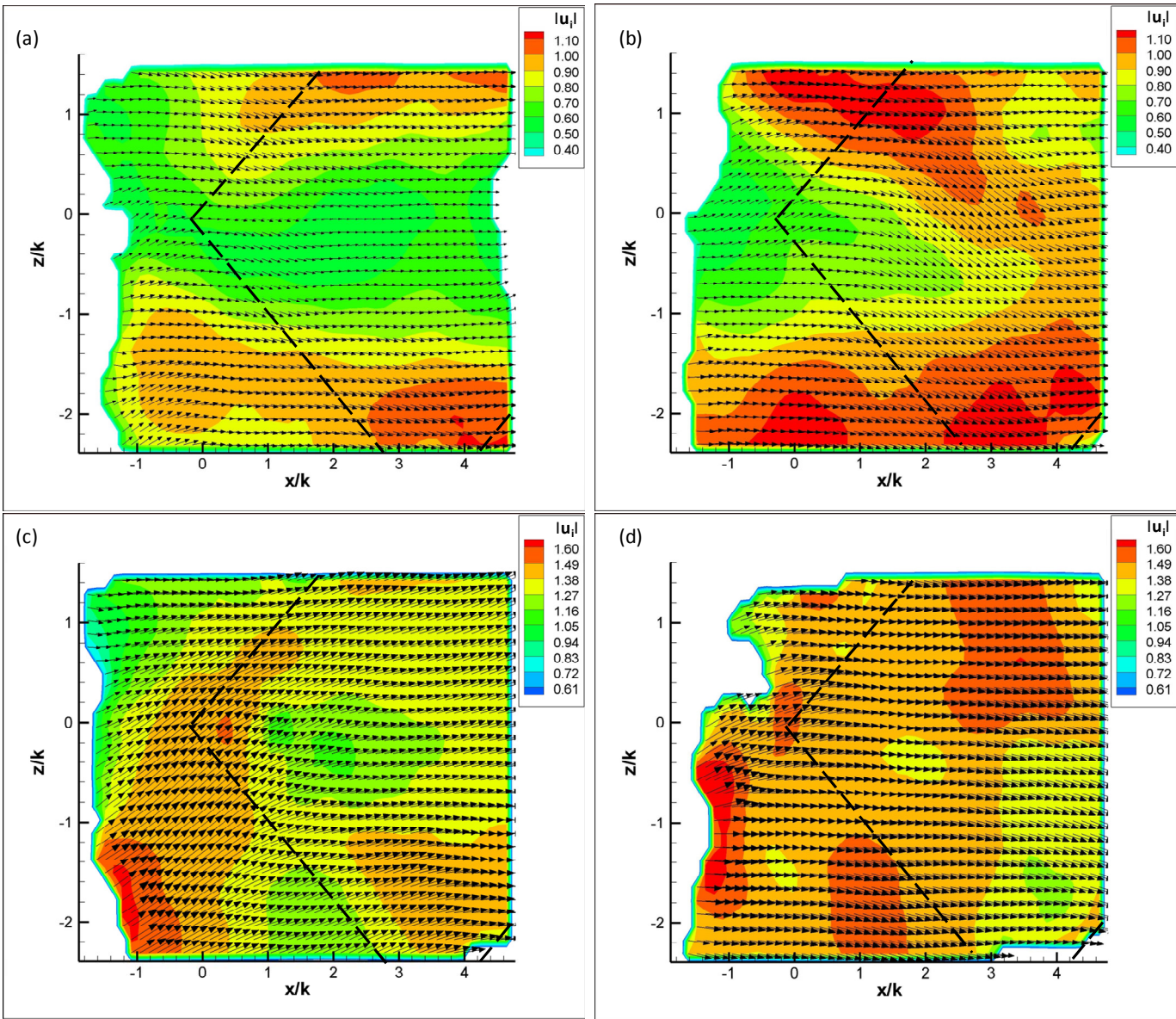
Fig. 6 Velocity vector maps and magnitude contour plots at: (a) and (b) $y/k = 0.07$, (c) and (d) $y/k = 1.27$. (a) and (c) correspond to the same instantaneous realization, and (b) and (d) correspond to a second realization. The velocity is presented in m/s, and the base of a pyramid is marked by dashed lines. Note the range for the contour is different for the different y locations.

4. CONCLUSIONS

Microscopic holographic PIV combined with optical index matching and local particle seeding enables us to measure the 3D volumetric velocity distributions in the inner part of a turbulent boundary layer over a rough wall, including the space between the roughness elements, i.e. $0.67<y/k<4.67$. In this paper, we present data obtained in a turbulent channel flow at $Re_\tau=3400$. The sample volume size is $460\times285\times285$ wall units, and the structured vector spacing is 8.5 wall units. It is obtained by spatial interpolation of 4000 - 5000 instantaneous unstructured vector measured using particle tracking. Due to the small number of hologram pairs analyzed to date (~40), we have only used the data for qualitative assessment of dominant structures. Iso-surfaces of Q demonstrate that the roughness

sublayer is flooded with quasi streamwise, slightly inclined vortices, of streamwise extents primarily between $1k$ and $2k$, consistent with vorticity distributions. The inclination angles of these structures are typically below 30º. Near the roughness elements, consistent with their shape, the velocity distributions show streamwise channeling with high velocity between the pyramid ridgelines, consistent with 2D PIV data (Hong et al., [7]). This phenomenon is confined to y/k<1.

The holographic data acquisition and analysis are still in progress. We plan to continue recording data with increasing resolution by improving the seeding procedures, and obtain sufficient realizations to perform statistical analysis of the observed structures, following, e.g. sampling tools described in Sheng et al. [20] for smooth wall boundary layers.
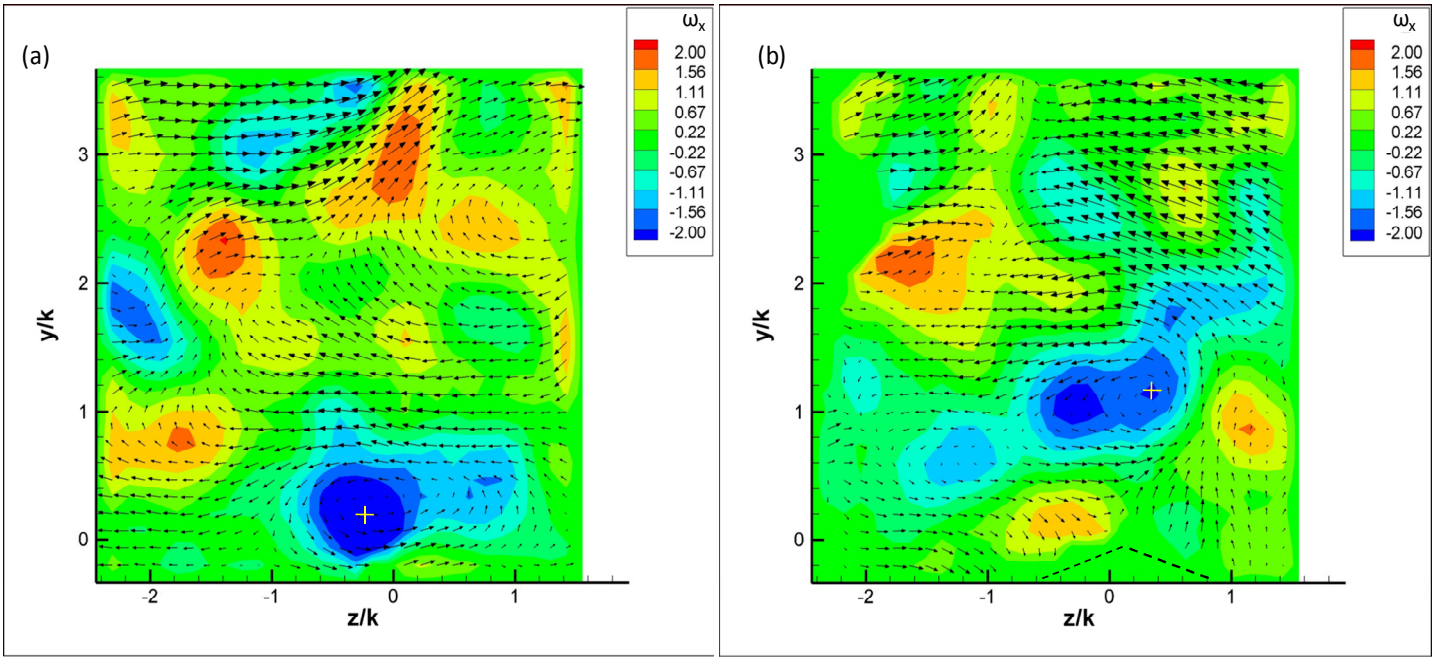
Fig. 7 Velocity vector maps and ω_x magnitude contours projected on the Y-Z planes at two different streamwise locations: (a) 0.83mm and (b) 1.83mm. The unit of ω_x is 10^3 s^{-1}. Dashed lines mark the outline of a pyramid cross-section.

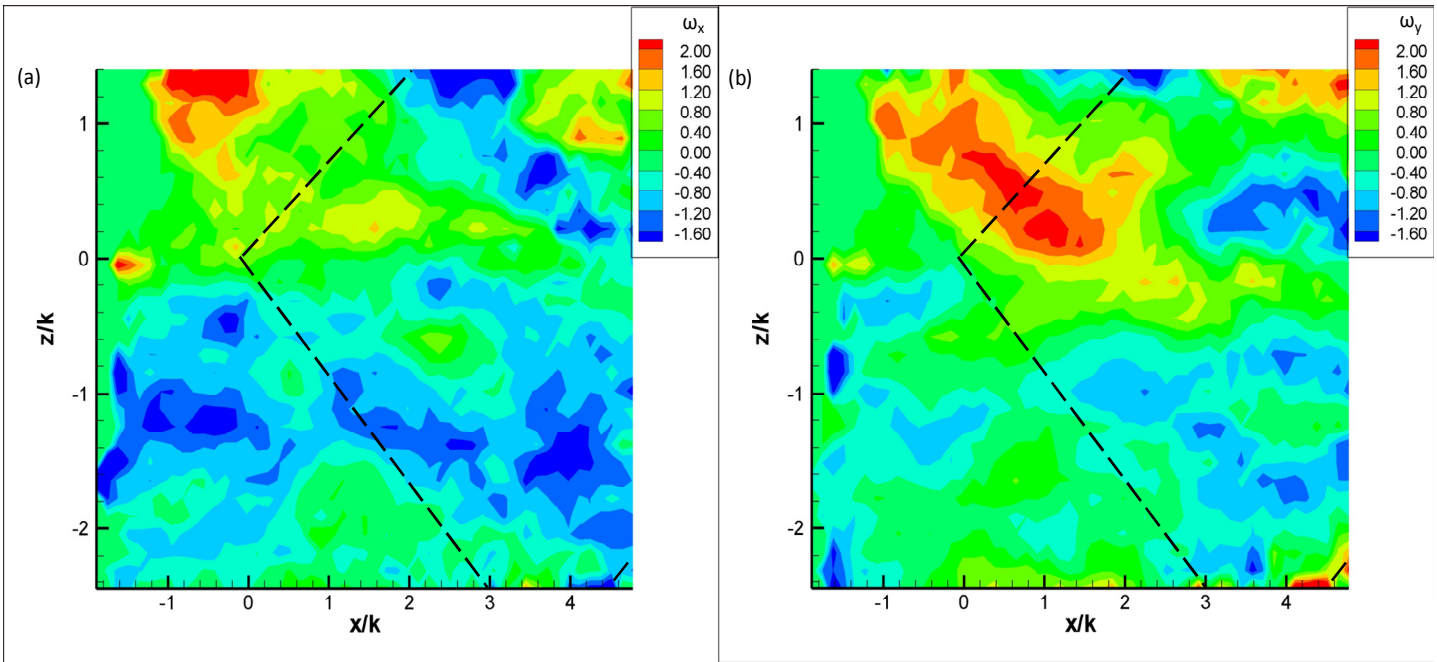Fig. 8 X-Z planes at y/k=1.07 showing (a)Contours of ω_x (b)Contours of ω_y. Regions with positive ω_x also have positive ω_y, pointing at streamwise inclined coherent structures. The unit of ω_x and ω_y is 10^3 s^{-1}. Dashed lines mark the base of a pyramid.
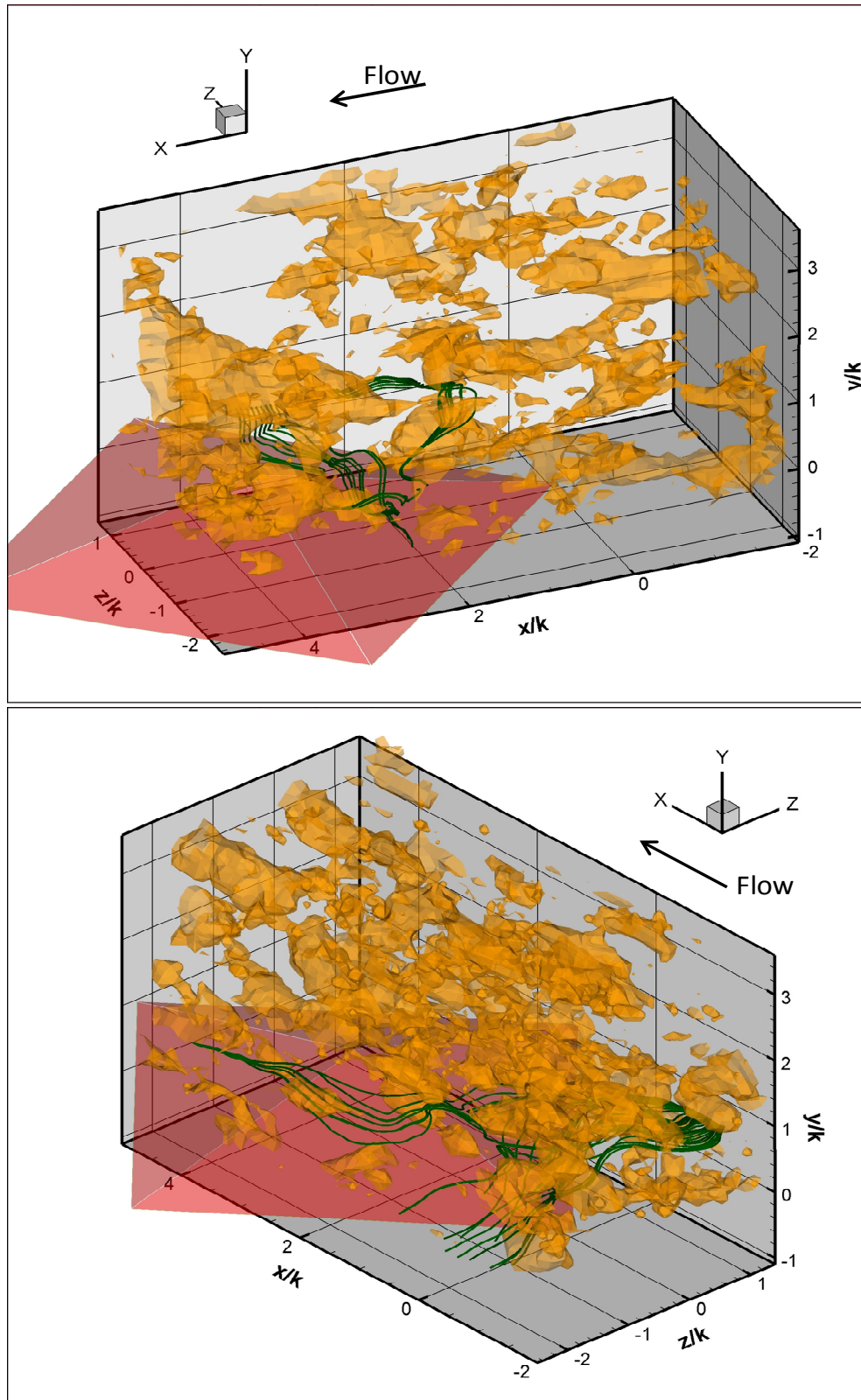
Fig. 9 Plots of iso-surfaces of $Q = 0.7 \times 10^6 \, s^{-2}$ along with vortex lines for two different instantaneous 3D vector maps. In (a), the vortex lines are lifted by the coherent structures close to the wall, (b) Some vortex lines bend towards the streamwise direction due presence of strong streamwise vortices in +x direction. A pyramidal roughness element is plotted to show its location.

5. REFERENCES

[1] Raupach M.R., Antonia T.A. & Rajagopalan S., 1991, "Rough wall boundary layers", *Applied Mechanics Review*, Vol. 44, pp. 1-25.

[2] Jimenez, J., 2004, "Turbulent flow over rough walls" *AnnualReview of Fluid Mechanics*, Vol. 36, pp. 173-196.

[3] Rotach, M.W., 1999, "On the influence of the urban roughness sublayer on turbulence and dispersion", *Atmospheric Environment*, Vol. 23, pp. 4001-4008.

[4] Aubry, N., Holmes P., Lumley J.L. & Emily Stone, 1988, "The dynamics of coherent structures in the wall region of a turbulent boundary layer", *Journal of Fluid Mechanics*, Vol. 192, pp. 115-173.

[5] Grass, A. J., 1971, "Structural features of turbulent flow over smooth and rough boundaries", *Journal of Fluid Mechanics,* Vol. 50, pp. 233-255.

[6] Krogstad, P.A., Antonia, R.A. & Browne L.W.B., 1992, "Comparison between rough and smooth wall turbulent boundary layers", *Journal of Fluid Mechanics*, Vol. 245, pp 599-617.

[7] Hong, J., Katz, J., Schultz, M.P., 2010, "Near-wall turbulence statistics and flow structures over 3D roughness in a turbulent channel flow", *Journal of Fluid Mechanics,* Submitted.

[8] Hong, J., Katz, J., Schultz, M.P., 2009, "High Resolution PIV Measurement near a Rough Wall in an Optically Index-matched Facility", *8TH Int. Symposium on particle Image Velocimetry*, pp. 247-250.

[9] Ikeda, T. & Durbin, P.A., 2002, "Direct Simulations of a Rough Wall Channel Flow", *Journal of Fluid Mechanics*, Vol. 571, pp. 235–263.

[10] Ashrafian, A., Andersson, H.I. & Manhart, M., 2004, "DNS of turbulent flow in a rod-roughened channel", *International Journal of Heat and Fluid Flow*, Vol. 25, pp. 373-383.

[11] Leonardi, S., Orlandi, P., Djenidi, L., Antonia, R.A., 2002, "DNS of a turbulent channel flow with different rough walls", *Advances in Turbulence IX*, pp. 387–90.

[12] Nakagawa, S. and Hanratty, T.J., 2001, "Particle image velocimetry measurements of flow over a wavy wall", *Physics of Fluids,* Vol. 13, 3504.

[13] Flack, K.A., Schultz, M.P., Shapiro, T.A., 2005, "Experimental support for Townsend's Reynolds number similarity hypothesis on rough walls", *Physics of Fluids*, Vol. 17, pp. 17-25.

[14] Wu, Y. & Christensen, K.T., 2007, "Outer layer similarity in presence of a practical rough wall topology" *Physics of Fluids*, Vol. 19, 085108.

[15] Krogstad, P.A. & Antonia, R.A., 1999, "Surface roughness effects in turbulent boundary layers", *Experiments in Fluids,* Vol. 27, pp. 450–60.

[16] Gabor, D., 1948, "A New Microscopic Principle", *Nature,* Vol. 161, pp. 777-778.

[17] Sheng J., Malkiel E. & Katz J., 2006, "Digital holographic microscope for measuring 3D particle distribution and motions", *Applied Optics*, Vol. 45, pp. 3893-3901.

[18] Sears, F.P., 1948, *Optics,* p. 248ff.

[19] Katz, J., Sheng, J., 2010, "Application of Holography in Fluid Mechanics and Particle Dynamics", *Annual Review of Fluid Mechanics,* Vol.32, pp. 531-555.

[20] Sheng, J., Malkiel, E. & Katz, J., 2009, "Buffer layer structures associated with extreme wall stress events in a smooth wall turbulent boundary layer", *Journal of Fluid Mechanics*, Vol. 633.

[21] Sheng, J., Malkiel, E. & Katz, J., 2008, "Using digital holographic microscopy for simultaneous measurements of 3D near wall velocity and wall shear stress in a turbulent boundary layer", *Experiments in fluids*, Vol. 45, pp. 1023-1035.

[22] Golub, G.H. & Loan, C. F, 1996, "The Singular Value Decomposition" and "Unitary Matrices" Ch. 2.5.3 and 2.5.6 in *Matrix Computations, 3rd ed*, pp. 70-71 and 73.

[23] Wu, H., Miorini, R. L., & Katz, J., 2010, "Measurements of the Tip Leakage Vortex Structures and Turbulence in the Meridional Plane of an Axial Water-Jet Pump", *submitted to Experiments in Fluids.*

[24] Hunt, J.C.R., Wray, A.A. & Moin, P., 1988, "Eddies, streams and convergence zones in Turbulent flows", *Center for Turbulence Research report,* CTR-S88, pp. 193-208.